Neurocomputing 552 (2023) 126512

Contents lists available at ScienceDirect

Neurocomputing

journal homepage: www.elsevier.com/locate/neucom

Edge-centric effective connection network based on muti-modal MRI for the diagnosis of Alzheimer's disease

Shunqi Zhang [a,1], Haiyan Zhao [b,1], Weiping Wang [a,c,*], Zhen Wang [e,d], Xiong Luo [a,c], Alexander Hramov [f,g], Jürgen Kurths [h,i]

[a] School of Computer and Communication Engineering, University of Science and Technology Beijing, Beijing 100083, China
[b] Department of Neurology, Peking University Third Hospital, Beijing 100191, China
[c] Shunde Innovation School, University of Science and Technology Beijing, Guangdong 528399, China
[d] School of Cyberspace, Northwestern Polytechnical University, Xian 710072, China
[e] School of Artificial Intelligence, Optics, and Electronics (iOPEN), Northwestern Polytechnical University, Xian 710072, China
[f] Center for Technologies in robotics and Mechatronics Components, Innopolis University, Innopolis 420500, Russia
[g] Saratov State Medical University, Saratov 410012, Russia
[h] Institute of Physics, Humboldt University of Berlin, Berlin 10099, Germany
[i] Potsdam Institute for Climate Impact Research, Potsdam 14473, Germany

ARTICLE INFO

Article history:
Received 20 March 2023
Revised 1 June 2023
Accepted 23 June 2023
Available online 10 July 2023
Communicated by Zidong Wang

MSC:
0000
1111

Keywords:
Alzheimer's disease diagnosis
Edge-centric effective connection network
Granger causality
Muti-modal MRI

ABSTRACT

Alzheimer's disease (AD) is an irreversible neurodegenerative disease. But if AD is detected early, it can greatly reduce the severity of the disease. Functional connection networks (FCNs) can be used for the early diagnosis of AD, but they are undirected graphs and lack the description of causal information. Moreover, most of FCNs take brain regions as nodes, and few studies have been carried out focusing on the connections of the brain network. Although effective connection networks (ECNs) are digraphs, they do not reflect the causal relationships between brain connections. Therefore, we innovatively propose an edge-centric ECN (EECN) to explore the causality of the co-fluctuating connection in brain networks. Firstly, the traditional conditional Granger causality (GC) method is improved for constructing ECNs based on the suppression relationship between structural connection network (SCN) and FCN. Then based on the improved GC method, edge time series and EECNs are constructed. Finally, we perform dichotomous tasks on four stages of AD to verify the accuracy of our proposed method. The results show that this method achieves good results in six classification tasks. Finally, we present some brain connections that may be essential for early AD classification tasks. This study may have a positive impact on the application of brain networks.

© 2023 Published by Elsevier B.V.

1. Introduction

As a progressive neurodegenerative disease, AD is the main type of senile dementia [1]. There are about 46 million AD patients in the world, and the increase is doubling in 20 years. It is estimated that the global number of AD patients will reach 130 million by 2050 [2]. With the deepening of research, we gradually realized that AD is a continuous development process, and the pathological changes of AD are much earlier than the appearance of clinical symptoms [3]. Mild cognitive impairment (MCI) is considered to be an intermediate stage between normal aging and AD. According to the course of the disease, the MCI stage can be divided into early MCI (EMCI) and late MCI (LMCI) [4]. In terms of the degree of disease, EMCI is more similar to NC, and LMCI is more similar to AD. Some neuroscientists believe that NC, EMCI, LMCI, and AD are the four major stages of AD, and accurate prediction and recognition of these four stages may be crucial.

With the progress of neuroimaging technology in recent years, Magnetic Resonance Imaging (MRI), Diffusion tensor imaging (DTI), Functional Magnetic Resonance Imaging (fMRI) and Positron Emission Computed Tomography (PET) and other imaging examinations can reveal the structural features and functional activity characteristics of the human brain in the early stage of disease [5]. Zeng et al. [6] proposed a new switching delayed particle

* Corresponding author at: School of Computer and Communication Engineering, University of Science and Technology Beijing, Beijing 100083, China.
E-mail address: weipingwangjt@ustb.edu.cn (W. Wang).

[1] These authors contributed equally to this work, and they are the first authors at the same time.

https://doi.org/10.1016/j.neucom.2023.126512
0925-2312/© 2023 Published by Elsevier B.V.

swarm optimization SVM method for the diagnosis of AD using MRI scans, and they gained satisfactory results. It is of great significance to study the early diagnosis of AD based on multimodal brain imaging data. Tatsuya et al. [7] used multi-modal MRI data to find the optimal machine learning model to classify EMCI and LMCI and achieved an accuracy of 70%. Based on MRI, Zeng et al. [8] proposed a novel deep belief network based multi-task learning algorithm developed for the classification AD/MCI and got good performance.

Blood oxygen-dependent level (BOLD) signal comes from resting-state functional magnetic resonance imaging (rs-fMRI) as a neurophysiological marker, which can capture changes in neuronal activity in the brain [9]. The two most important elements of the brain network are nodes and connections. Different definitions of these two elements often lead to great changes in the function and structure of the corresponding brain network. Thus, brain functional and structural patterns and their potential correlations can be demonstrated from different perspectives, providing different ideas for the analysis of brain diseases [10,11]. Therefore, it has become a hot issue in recent years to study the differences in brain networks between AD and MCI subjects and normal subjects by constructing brain networks based on neuroimaging data [12]. At present, the mainstream brain networks include FCN, SCN, ECN, and so on. SCN and FCN are essentially undirected graphs, which have been regarded as important biomarkers and received much research attention. Ibrahim et al. [13] determined the diagnostic capability of rs-fMRI in identifying FCN abnormalities in the DMN of AD or MCI patients by machine learning methods. Zhao et al. [14] proposed a regional radiomics similarity network based on SCN for subtype analysis of MCI, which provides a good basis for the accurate identification of early AD. Zhang et al. [15] combined fMRI, MRI and DTI to construct deep brain connectome to simulate SCN and FCN, and achieved an accuracy of 92.7% on the ADNI dataset. Some scholars believe that SCN and FCN can only indicate whether there is a connection relationship between brain regions and the strength of the connection relationship, without directionality. Furthermore, the current common brain connection network is often node-centered, that is, nodes represent brain regions while edges mean the connection strength relationship between brain regions. Recently, Faskowitz et al. [16] proposed edge-centric FCN (EFCN) based on fMRI. The nodes of EFCNs represent the functional connection of brain regions, and the edges represent the degree of correlation between the connections of some two brain regions and the connections of the other two brain regions. EFCN can be seen as a supplement and extension of the traditional node-centric representation of FCNs. EFCN reveals how communication between different brain regions evolves over time and seems to reflect co-fluctuations in ROIs. However, EFCN is also an undirected graph, which cannot obtain the causal relationship between brain region fluctuations.

ECN, as a directed graph, can represent the causal effect information of the connection relationship between neural signals in the brain, which is more biologically interpretable [17]. Zhao et al. [18] proposed to detect the number and position of rapid connection changes from a BOLD sequence, and then estimated the effective connection network using the conditional Granger causality method. Then they applied it to the classification task of AD/NC and achieved an accuracy of 86.24%. Dang et al. [19] constructed ECN using dynamic Bayesian networks for DTI and fMRI, and proved its effectiveness in synthetic data. Ji et al. [20] proposed a brain-effect connection ant colony learning method combining fMRI and DTI. They applied it to simulation data sets and real fMRI-DTI data sets for verification and achieved good results. Their results also showed that combined multi-modal brain imaging was better than single-modal brain imaging. However, when the ECN is constructed by the traditional GC method, the ECN is often not robust and accurate enough. Because the traditional GC method is not good at distinguishing direct and indirect causal relationships, it is easy to identify false positive associations [21,22].

Therefore, although FCN and SCN are widely used in AD diagnostic tasks, they are essentially undirected graphs, lacking the description of causal information. Although ECNs are digraphs, they may have low accuracy when constructing ECNs like the traditional Granger causality method. In addition, there is a lack of research on the causal transmission of brain regions. To solve the above problems, we first improve the traditional Granger method based on the inhibition relationship of SCN to ECN. Then, a new EECN model is proposed to explore the causal relationship of the co-fluctuating connectivity of brain networks. The overall structure of EECN is similar to EFCN, but the edges of EECN represent causal relationships between connections between two ROIs and connections between two other ROIs. In other words, the EECN model can help us understand the causal transmission between two brain connections in the brain. And High EECN values indicate the strong causal relationship between the co-fluctuations of the two edges in time, while low EECN values indicate the basically independent co-fluctuation causal pattern. Finally, we verify the proposed EECN method in the classification tasks of AD, LMCI, EMCI, and NC. We depict the process in Fig. 1. Our main contributions are as follows:

1. Based on the principle of the GC method in constructing ECN, this paper introduces the constraint relation between SCN and ECN to improve the traditional conditional Granger method.
2. We construct edge time series based on the BOLD time series and then use the improved GC method to construct EECN.
3. This EECN method is applied to six binary classification tasks in four stages of NC, EMCI, LMCI, and AD, and achieves better performance than traditional methods.

2. Materials and Methods

2.1. Preparations for the construction of edge-centric effective connection network

In brain science, the brain network is often regarded as a simple mapping of the brain, and neurons and their pairwise interactions are regarded as nodes and edges of the network respectively. The model is usually node-centric because it regards neurons (or regions of the brain) as the basic units of brain structure and function. The model generally focuses on the analysis of the attributes of nodes or node groups and is generally interpreted as a measure of inter-area communication. However, as a low-order brain network, the node-centric brain network construction method cannot capture the potential connections between edges. Faskowitz et al. [16] proposed to study brain functional networks from the perspective of connecting edge centric. The method is used to estimate the strength of the functional connection between pairs of brain regions. Thus we develop interpretable time series for each pair of connected edges to illustrate the fluctuation of its weight over time. A high EFCN indicates a strong similarity in the co-fluctuations of the two edges in time, while a low EFCN indicates an essentially independent co-fluctuation pattern. EFCN is more reflective of how communication between different brain regions has evolved over time.

In order to construct an edge-centric brain network, it is necessary to get the edge time series. Assuming the number of subjects is M, the BOLD time series of the $m-th$ subject is described as $S^m \in \mathbb{R}_{N\times T}(m = 1, 2, \ldots, M)$ where N and T, respectively, represent the number of brain regions and the length of time signals series.

Let $s_i = [s_i(1), s_i(2), \ldots, s_i(T)], s_j = [s_j(1), s_j(2), \ldots, s_j(T)] \in S^m$ where i and j respectively means the $i-th$ and $j-th$ ROI in the

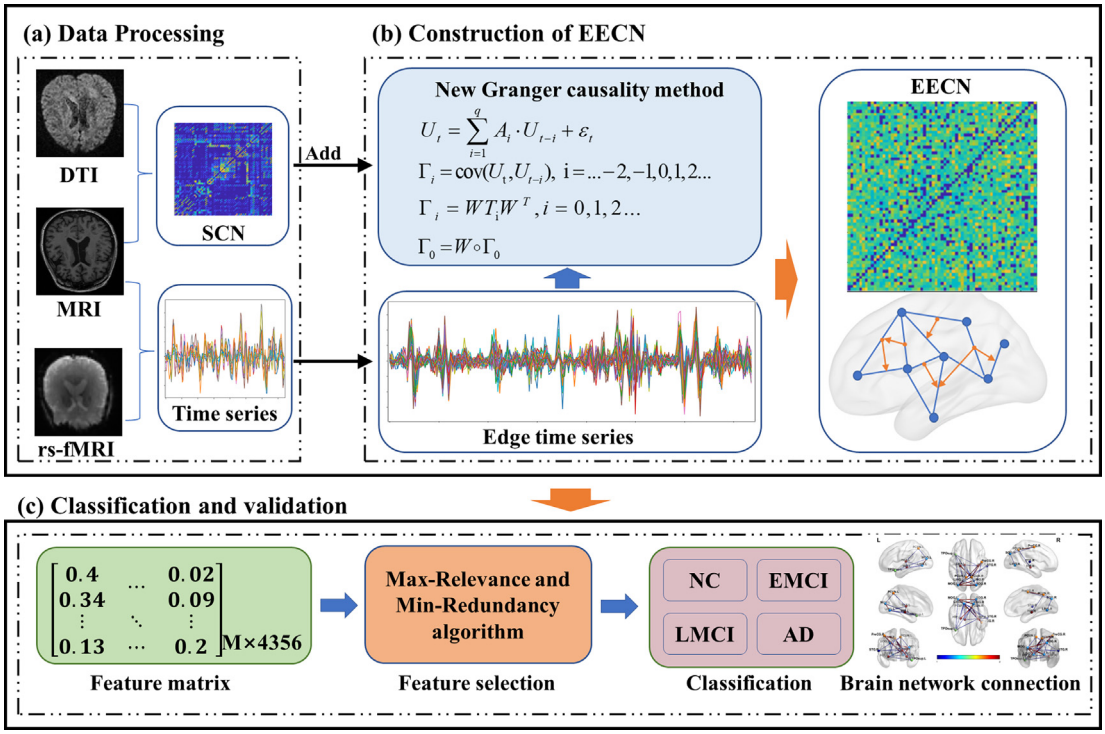

Fig. 1. The flowchart of the proposed framework for EECN analysis. (a) shows the using multi-modal data including MRI, fMRI, and DTI. SCN and BOLD time series are obtained after data processing. (b) shows the framework structure diagram according to the proposed EECN method. (c) shows the process of feature construction and feature selection of EECN, classification, and brain network connection selection.

brain network. Then, we possess s_i and s_j using z-score, and calculate their pairwise products:

$$\begin{aligned} R_i &= zscore(s_i), \\ R_j &= zscore(s_j), \\ X_{ij} &= \tfrac{1}{T}\sum_t [R_i(t) \cdot R_j(t)], \end{aligned} \tag{1}$$

$$\mathrm{EFCN}_{\mathrm{ij,uv}} = \frac{\sum_t \mathrm{X_{ij}(t)} \cdot \mathrm{X_{uv}(t)}}{\sqrt{\sum_t \mathrm{X_{ij}}(t)^2}\sqrt{\sum_t \mathrm{X_{uv}}(t)^2}}, \tag{2}$$

where X_{ij} is the resulting product pair time series, which we call the edge time series in this paper. EFCN is the obtained edge functional connection network. The network node of EFCN represents the connection strength of i-th ROI and j-th ROI, and the edge represents the co-fluctuation of the two connecting edges of ROI i and j, ROI u and v, that is, the connection association between i and j, u and v.

Corresponding to EECN, we construct the edge-centric SCN, the details are as follows:

$$\mathrm{W}_{ij,uv} = \begin{cases} 0, & \text{if} \quad \mathrm{SC_{ij}} = 0 \quad \text{or} \quad \mathrm{SC_{uv}} = 0; \\ \max(SC_{ij}, SC_{uv}), & \text{otherwise.} \end{cases} \tag{3}$$

where SC means the SCN after the preprocessing of the subject's brain image data, and i, j, u, and v represent the index number of the brain region. W represents the edge-centric SCN corresponding to EECN, and W is a symmetric matrix. In order to avoid the problem of matrix irreversibility caused by a singular matrix, noise with values between $[10^{-3}, 10^{-4}]$ is added to W, and then W is symmetrized.

2.2. Improved Granger causality method

2.2.1. Traditional Granger causality method

GC model is an analytical approach based on the vector autoregressive model, which combines the values of past time series linearly to indicate the values of current time series [23]. It is often used to test causality in time series data. Through the analysis of the brain network, it can reflect the direction of information transmission between brain regions or neurons. In general, for two stationary time series x_t and $y_t (t = 1, 2, \ldots t)$, for predicting the current value of x, if only using historical information of x is less instrumental than the combination of historical information of x and y, that is, the error of the latter gets declined. Then we can believe y could be the Granger cause of x. The traditional GC test only involves a causality test between two variables, and the equation is as follows:

$$x_t = \sum_{i=1}^{q} a_{1i} x_{t-i} + \varepsilon_{1t}, \tag{4}$$

$$x_t = \sum_{i=1}^{q} a_{2i} x_{t-i} + \sum_{i=1}^{q} b_{2i} y_{t-i} + \varepsilon_{2t}, \tag{5}$$

where q is the model order, that is the maximum number of lagged samples, which is determined by the Akaike Information Criterion (AIC) [24]. a_{1i}, a_{2i}, b_{2i} are the model coefficient, ε_{1t} and ε_{2t} mean the random error term independent of time.

The Granger causality of y to x is defined as follows:

$$F_{y \to x} = \ln \frac{\mathrm{var}(\varepsilon_{1t})}{\mathrm{var}(\varepsilon_{2t})}, \tag{6}$$

when $\mathrm{var}(\varepsilon_{1t}) > \mathrm{var}(\varepsilon_{2t})$, we believe that the past value of y can improve the result of prediction, $F_{y \to x} > 0$ at this time. In addition, we can verify whether the value of GC is meaningful by F-test.

2.2.2. Improved conditional Granger causality method

In general, traditional GC methods do not perform well in distinguishing direct causality from indirect causality. Therefore, Faes et al. [22] introduced a new stationary variable z and proposed conditional Granger causality (CGC) method based on the traditional GC method.

In order to make the constructed brain network more accurately reflect the directionality of information transmission between brain regions, we introduce the constraint relationship between SCN and FCN into CGC. Specifically, the SCN generated by MRI and DTI is processed to obtain edge-centric SCN, and the edge-centric will be introduced into CGC as a parameter matrix. The specific model is as follows:

Let U be a multivariate stationary time series,

$$U_t = \sum_{i=1}^{q} A_i \cdot U_{t-i} + \varepsilon_t \tag{7}$$

$$\Gamma_i = \mathrm{cov}(U_t, U_{t-i}), \mathrm{i} = \ldots -2, -1, 0, 1, 2 \ldots \tag{8}$$

where Γ_i represents the autocovariance matrix of U_t, A_i represents the regression coefficient, q means model order, and ε_t represents error. Since the ECN is essentially FCN, SCN still has a limiting effect on it. Then we introduce the edge-centric SCN as a parameter matrix,

$$\Gamma_i = W\Gamma_i W^T, i = 0, 1, 2 \ldots \tag{9}$$

$$\Gamma_0 = W \circ \Gamma_0 \tag{10}$$

According to the Yule-Walker equations [25], we could obtain

$$(\Gamma_1 \ldots \Gamma_q) = (A_1 \ldots A_q)\Gamma_0 \tag{11}$$

$$(A_1 \ldots A_q) = (\Gamma_1 \ldots \Gamma_q)(\Gamma_0)^{-1} \tag{12}$$

$$\varepsilon_t = U_t - \sum_{i=1}^{q} A_i \cdot U_{t-i} \tag{13}$$

Specifically, let x, y, and z be subsets of the multivariate stationary time series U,

$$U = \begin{pmatrix} x \\ y \\ z \end{pmatrix} \tag{14}$$

The Granger causality model is as follows:

$$x_t = \sum_{i=1}^{q} a_{3i} x_{t-i} + \sum_{i=1}^{q} c_{3i} z_{t-i} + \varepsilon_{3t}, \tag{15}$$

$$x_t = \sum_{i=1}^{q} a_{4i} x_{t-i} + \sum_{i=1}^{q} b_{4i} y_{t-i} + \sum_{i=1}^{q} c_{4i} z_{t-i} + \varepsilon_{4t} \tag{16}$$

Similar to traditional GC, x, y and z are stationary time series, a_{3i}, c_{3i}, a_{4i} and b_{4i} and c_{4i} are model coefficients, ε_{3t} and ε_{4t} are random error terms independent of time.

When given z, the CGC from y to x conditional on z is:

$$F_{y \to x|z} = \ln \frac{\mathrm{var}(\varepsilon_{3t})}{\mathrm{var}(\varepsilon_{4t})} \tag{17}$$

If $\mathrm{var}(\varepsilon_{3t}) > \mathrm{var}(\varepsilon_{4t})$, we believe that under the condition of z, the introduction of y variable improves the prediction of x value, and then $F_{y \to x|z} > 0$. When the GC between x and y is completely mediated by z, then $b_{4t} \equiv 0$ and $\mathrm{var}(\varepsilon_{3t}) = \mathrm{var}(\varepsilon_{4t})$, so $F_{y \to x|z} \equiv 0$. Whether causality is meaningful can also be verified by the F-test.

By substituting the constructed edge time series and edge-centric SCN into the improved Granger method, an EECN can be obtained. Its nodes represent connections between two ROIs. Its edges indicate a causal relationship between a connection between two ROIs and a connection between two other ROIs, which is directed. The size of the EECN is $\frac{N(N-1)}{2} \times \frac{N(N-1)}{2}$.

Algorithm 1: Algorithm flow for the improved Granger causality method.

Input: U_t, $t = \ldots -2, -1, 0, 1, 2 \ldots$; q; W
Output: F
for $i = 1$ *to* q **do**
  $\Gamma_i = \mathrm{cov}\ (U_t, U_{t-i})$;
  Update Γ_i based on Eq.(9);
end
Update Γ_0 based on Eq.(10);
Compute ε_t based on Eq.(11, 12,13);
Compute F based on Eq.(17);
return F

3. Experiments and results

3.1. Data collection

Three modalities of brain imaging data in the Alzheimer's disease neuroimaging initiative (ADNI) [26] dataset (https://adni.loni.usc.edu) are conjointly analyzed in this work, including MRI, rs-fMRI, and DTI. ADNI enables researchers around the world to share data about the early stage of AD. The goal of ADNI is to study MCI and AD intervention, prevention, and treatment by using different biomarkers. We select 173 subjects that have all three modalities, including 52 patients with EMCI (average age 75.8 years, 22 male and 30 female), 30 patients with LMCI (average age 77.4 years, 20 male and 10 female), 34 patients with AD (average age 74.7 years, 19 male and 15 female) and 57 age-matched NC (average age 72.2 years, 32 male and 25 female). The details of demographics and clinical characteristics are described in Table 1.

3.2. Data Description and Preprocessing

3.2.1. Data Description

The MRI data has field strength = 3.0 Tesla, FA = 90.0°, matrix = 240.0 × 256.0 × 176.0, slice thickness = 1.0 mm, pixel spacing = 1.0 × 1.0 mm and TR = 2300 ms. The DTI data has strength = 3.0 Tesla, FA = 90.0°, gradient directions = 54.0, matrix = 1044.0 × 1044.0 × 55.0, pixel spacing = 1.0 × 1.0mm, slice thickness = 2.0 mm, and TR/TE = 7200/56 ms. The rs-fMRI data has field strength = 3.0 Tesla, slice thickness = 3.4 mm, FA = 90.0°, matrix = 448 × 448, pixel spacing = 3.4 × 3.4mm and TR/TE = 3000.0/30.0 ms. Subjects are required to keep their eyes open, and remain relaxed and awake during the scan.

Table 1
Demographic and Clinical Characteristics of Subjects.

Group	Number	Male/Female	Age(Mean ± SD)
NC	57	32/25	72.2 ± 6.9
EMCI	52	22/30	75.7 ± 6.8
LMCI	30	20/10	77.4 ± 6.3
AD	34	19/15	74.7 ± 6.1

3.2.2. Data Preprocessing

We convert these three images to neuroimaging informatics technology initiative (NIfTI) file format. For the structure images, we use the PANDA toolbox and FreeSurfer V6.00 to perform image preprocessing steps. For MRI, we carry out skull removal operations. Then, to eliminate the noise during scanning, the head motion correction operation is carried out. In order to avoid the influence of different subjects' brain sizes, we carry out the spatial standardization operation. To further eliminate the noise of the subject scanning, spatial smoothing, and filtering are carried out. Finally, the Anatomical Automatic Labeling (AAL) template [27] is applied to segment the brain space into 90 ROIs. The MRI images are used as templates for DTI and fMRI processes. For DTI images, we do format conversion first. Then we do skull removal and correct the head motion. We do the eddy current correction to alleviate the vortex distortion image. We calculate the Fractional Anisotropy (FA) of each voxel, register the FA image with the corresponding processed MRI, and use the AAL map in the standard space for segmentation. The cerebral cortex surface is divided into 90 regions, and each one is defined as a brain network node. Finally, the structural connection network of each subject is obtained. For rs-fMRI images, we preprocess them through DPARSF [28] toolbox (http://rfmri.org/DPARSF). To eliminate the effect of noise generated by the subject's adaptation process during the initial scan, we delete the first 10 time points for each subject. We conduct the steps including slice timing correction, register MRI to rs-fMRI, motion rectification, normalization, smoothing, and bandpass filtering. Then we segment the brain space into 90 ROIs. At last, the time series of each subject is acquired from the BOLD signals of all voxels.

3.3. Brain network regions selection

In this paper, we select 12 brain regions related to AD as ROIs corresponding to the AAL template [27]. It includes right Precentral gyrus, left Hippocampus, right Hippocampus, left Lingual gyrus, right Lingual gyrus, right Superior occipital gyrus, left Middle occipital gyrus, left Precuneus, right Precuneus, left Thalamus, right Superior temporal gyrus, left Temporal pole: superior temporal gyrus. We list and show them in Table 2 and Fig. 2.

3.4. Feature extraction/selection

We obtained the EECNs of all subjects in the four stages of AD, LMCI, EMCI, and NC by the above method, and then we need to extract useful features from the EECNs to effectively identify subjects in the four states. Using the connection weight of the network as the feature can avoid the influence of different kinds of features on the experimental results, so we choose to use the connection weight of EECN as the feature. The overall feature extraction process is similar to FCN, but since EECN is an asymmetric graph, all its connected edges need to be used as feature sets. If the number of ROIs is N, the number of nodes in the EECN should be $N(N-1)/2$, and there are $N^2(N-1)^2/4$ edges. In order to solve the problem of high-dimensional data, we use the mRMR method [29] to select the features with the best compromise ability between redundancy and correlation.

Table 2
List of selected ROI names

No.	ROI
1	R.Precentral gyrus
2	L.Hippocampus
3	R.Hippocampus
4	L.Lingual gyrus
5	R.Lingual gyrus
6	R.Superior occipital gyrus
7	L.Middle occipital gyrus
8	L.Precuneus
9	R.Precuneus
10	L.Thalamus
11	R.Superior temporal gyrus
12	L.Temporal pole: superior temporal gyrus

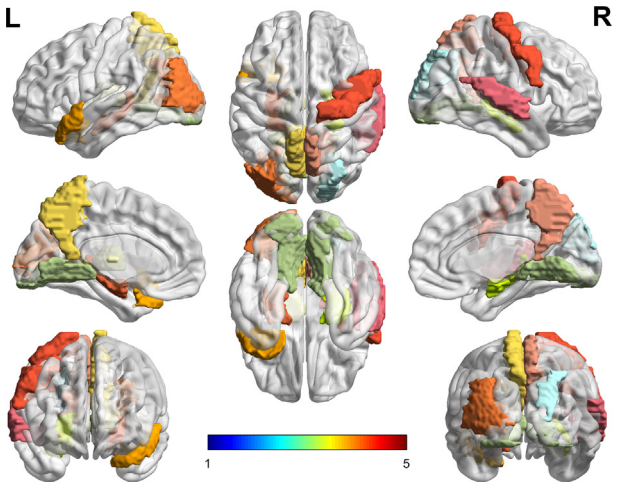

Fig. 2. The distribution of the 12 selected ROIs in the brain.

3.5. Experimental setting

In our experiments, we adopt the 10-fold cross-validation strategy. In order to reduce the experimental error, we repeat 200 times for all methods and calculate the average results as the final results. We evaluated the performance using the support vector machine (SVM) as a baseline test. Accuracy (ACC), sensitivity (SEN), specificity (SPE), F1score (F1), and the area under the receiver operating characteristic curve (AUC) are employed to measure the performance in classification. They can be calculated as follows:

$$ACC = \frac{TP + TN}{TP + TN + FN + FP}, \tag{18}$$

$$PPV = \frac{TP}{TP + FP}, \tag{19}$$

$$SEN = \frac{TP}{TP + FN}, \tag{20}$$

$$SPE = \frac{TN}{TN + FP}, \tag{21}$$

$$BAC = \frac{SEN + SPE}{2}, \tag{22}$$

$$F1 = \frac{2 \cdot PPV \cdot SEN}{PPV + SEN}, \tag{23}$$

where TP means true positive, TN means true negative, FP means false positive, and FN means false negative respectively. AUC is defined as the area under the ROC curve and the coordinate axis.

We take different effect network constructions as comparison methods, mainly including node-centered ECN (NECN) based on traditional GC method, NECN (NECN_SC) by improved GC construction proposed in this paper, edge-centered ECN (EECN) built by traditional GC method and edge time series, and EECN (EECN_SC)

built by improved GC proposed in this paper. In addition, logistic regression (LR) [30] and random forest (RF) [31] are used to conduct auxiliary comparative experiments to verify the effectiveness of our proposed method. Six classification tasks are performed to evaluate the performance, including (1) NC vs. EMCI classification. (2) NC vs. LMCI classification. (3) NC vs. AD classification. (4) EMCI vs. LMCI classification. (5) EMCI vs. AD classification. (6) LMCI vs. AD classification.

3.6. Classification results using different methods

Based on NECN, NECN_SC, EECN, and EECN_SC, we repeated 200 experiments in six dichotomous tasks of NC, EMCI, LMCI, and AD, and the final results are averaged. Table 3 summarizes the performance of the above four methods on all classification tasks.

(1) In the classification task of NC and EMCI, the accuracy of NECN, NECN_SC, EECN, and EECN_SC are 70.45%, 71.49%, 90.86%, and 91.52% respectively. The balanced accuracy is 0.7108,0.7179, 0.9086 and 0.9196, respectively. AUCs are 0.7751, 0787, 0949, 0.9705, and F1 scores are 0.711, 0.7086, 0.9083, and 0.9108, respectively. Compared with NECN, the ACC, BAC, and AUC of NECN_SC are slightly improved, but the F1 score is slightly worse. And all indexes of EECN_SC are slightly better than those of EECN except SEN. Compared with Node-centric ECN, edge-centric ECN has significant improvement in all our indicators. Compared with NECN, the ACC, BAC, and AUC of NECN_SC are slightly improved, but the F1 score is slightly worse. Compared with NECN, the ACC, BAC, and AUC of NECN_SC are slightly improved, but the F1 score is slightly worse. All indexes of EECN_SC are slightly better than those of EECN except SEN. Compared with NECN, the ACC, BAC, and AUC of NECN_SC are slightly improved, but the F1 score is slightly worse. All indexes of EECN_SC are slightly better than those of EECN except SEN. Compared with node-centric ECN, edge-centric ECN has significant improvement in all aspects. (2) In the classification task of NC and LMCI, the accuracy of NECN method is 71.71%. After using the improved GC, the accuracy of NECN_SC method was 83.32%, which is increased by 11.61%. Moreover, compared with NECN, BAC of NECN_SC increased by 0.1369, AUC increased by 0.0767, and F1 score increased by 0.0823. After the introduction of EECN, the ACC of EECN and EECN_SC increased by 0.2126 and 0.1186, BAC increases by 0.2716 and 0.1476, AUC increases by 0.1876 and 1158, compared with NECN and NECN_SC, respectively. F1 score increased by 0.1473 and 0.087. Compared with the classification task (1), the performance of the task (2) is generally better, that is, LMCI is more distinguishable from NC than EMCI. (3) In the classification task of EMCI and LMCI, the accuracy of NECN method is 71.96%. After using the improved GC, the accuracy of NECN_SC method is 77.28%, which is increased by 5.32%. EECN_SC performs better than EECN, with the accuracy increased by 2.49%, and other indicators are also improved. (4) In the classification task of NC and AD, after using the improved GC, the accuracy of NECN_SC reaches 87.44%, which is 11.8% higher than that of NECN, and the accuracy of EECN_SC reaches 98.3%. The accuracy of EECN is 3.82% higher than that of EECN. And in other indicators, the method using improved GC is significantly better than the original GC method. As in the previous task, EECN and NECN, EECN_SC and NECN_SC are significantly improved. In addition, compared with task (1) and task (2), the performance of all methods in task (4) is better, which indicates that the proposed brain network can better analyze and diagnose the differences between NC, EMCI, LMCI and AD, indicating the effectiveness of the proposed method. (5) In the classification task of EMCI and AD, the accuracy of NECN_SC is 11.34% higher than that of NECN, BAC increased by 0.0935, AUC increased by 0.1093, and F1 score increased by 0.1716. In this classification task, the best performance is still the proposed EECN_SC, the accuracy is 96.26%, BAC is 0.9558, AUC is 0.9904, F1 is 0.9657. (6) In the classification task of EMCI and LMCI, the classification accuracy of EECN_SC is 26.9% higher than that of NECN, 12.7% higher than that of NECN_SC, and 6.23% higher than that of EECN.

Moreover, for the six classified tasks, we first compare them based on NECN, NECN_SC, EECN, and EECN_SC. It can be seen that the EECN_SC proposed in this paper has achieved the best results in the six classification tasks, and the improvement is more obvious than the traditional NECN method. However, the results of the same method on the six classification tasks differ greatly, so the difficulty of the six classification tasks may be different. It can be seen from the results that the classification task of NC and AD can get better performance than other groups. The stage of AD can be divided into NC, EMCI, LMCI, and AD according to the severity of the disease. NC and EMCI are closer, and LMCI and AD

Table 3
The performance of the four methods on six classification tasks, and the boldface indicates the optimal value in a certain classification task.

Task	Method	ACC	PPV	SEN	SPE	BAC	AUC	F1
NC vs EMCI	NECN	0.7045	0.7097	0.7585	0.663	0.7108	0.7751	0.711
	NECN_SC	0.7149	0.7348	0.7232	0.7126	0.7179	0.787	0.7086
	EECN	0.9086	0.8974	**0.9351**	0.8822	0.9086	0.949	0.9083
	EECN_SC	**0.9152**	**0.9457**	0.8937	**0.9454**	**0.9196**	**0.9705**	**0.9108**
NC vs LMCI	NECN	0.7171	0.7445	0.8786	0.4224	0.6505	0.7946	0.7903
	NECN_SC	0.8332	0.8303	0.9422	0.6245	0.7834	0.8713	0.8726
	EECN	0.9297	**0.953**	0.9346	**0.9095**	0.9221	0.9822	0.9376
	EECN_SC	**0.9518**	0.9464	**0.9808**	0.8812	**0.931**	**0.9871**	**0.9596**
EMCI vs LMCI	NECN	0.7196	0.7228	0.9122	0.419	0.6656	0.8104	0.7917
	NECN_SC	0.7728	0.7588	0.9486	0.4725	0.7106	0.8449	0.8301
	EECN	0.9104	0.8966	0.9736	0.777	0.8753	0.9489	0.9275
	EECN_SC	**0.9353**	**0.9217**	**0.983**	**0.8333**	**0.9082**	**0.9812**	**0.9468**
NC vs AD	NECN	0.7564	0.7751	0.8815	0.5458	0.7137	0.8687	0.808
	NECN_SC	0.8744	0.8847	0.9221	0.7918	0.8569	0.9519	0.8946
	EECN	0.9457	0.9466	0.9088	0.9651	0.9369	0.984	0.9175
	EECN_SC	**0.9839**	**0.982**	**0.9537**	**0.9945**	**0.9741**	**1**	**0.9718**
EMCI vs AD	NECN	0.7464	0.72	0.7703	0.7301	0.7502	0.8053	0.7082
	NECN_SC	0.8598	0.8561	0.9263	0.7612	0.8437	0.9146	0.8798
	EECN	0.9321	0.9296	0.9619	0.8782	0.9201	0.9835	0.9397
	EECN_SC	**0.9626**	**0.9585**	**0.9798**	**0.9319**	**0.9558**	**0.9904**	**0.9657**
LMCI vs AD	NECN	0.6911	0.7587	0.735	0.6383	0.6866	0.81	0.7228
	NECN_SC	0.8331	0.8349	0.7849	0.8696	0.8273	0.9069	0.7827
	EECN	0.8978	0.9054	0.938	0.8275	0.8827	0.962	0.9139
	EECN_SC	**0.9601**	**0.9634**	**0.9762**	**0.9298**	**0.953**	**0.9886**	**0.9669**

are closer. Therefore, the brain networks of NC and AD groups are more different, so the differentiation is greater and the classification performance is the best. Similarly, compared with the LMCI group, the NC group, and the EMCI group has greater differentiation and better classification performance.

In particular, we plot the ROC curves of these four methods in six classification tasks, as shown in Fig. 3. The statistical bar charts of each evaluation index are depicted in Fig. 5.

In order to further verify the robustness of the proposed method (EECN_SC), we select SVM, LR and RF as classifiers to do comparative experiments. Specifically, we conduct 200 comparative experiments on each of the six classification tasks and finally take their average values. The details are shown in Table 4. We select ACC, AUC and F1 score as the main indicators and plot their results in Fig. 4.

Moreover, we also compare the proposed method with other recent algorithms related to AD diagnosis, and the results are shown in Table 5. It can be seen that the proposed method generally achieves better performance than other methods, demonstrating the effectiveness of the proposed EECN_SC method in the early diagnosis of AD.

4. Discussion

In this paper, we propose a new framework for the construction of EECN. EECN acts as a directed graph, where nodes represent the connections of two ROIs and edges represent the fluctuating causal relationships between two ROIs and the connections of two other ROIs. It can help us to understand how communication between different brain regions evolves.

In particular, to solve the problem of the low accuracy of the traditional CGC method in constructing ECNs, we introduce the SCN to FCN constraint relationship and improved the traditional CGC method. The comparison experiments demonstrate that the performance of the improved CGC method is better than the original method. Then we process the BOLD time series into edge time series, and then use the new CGC method to construct EECNs of NC, EMCI, LMCI, and AD. The constructed EECN is described in Fig. 6.

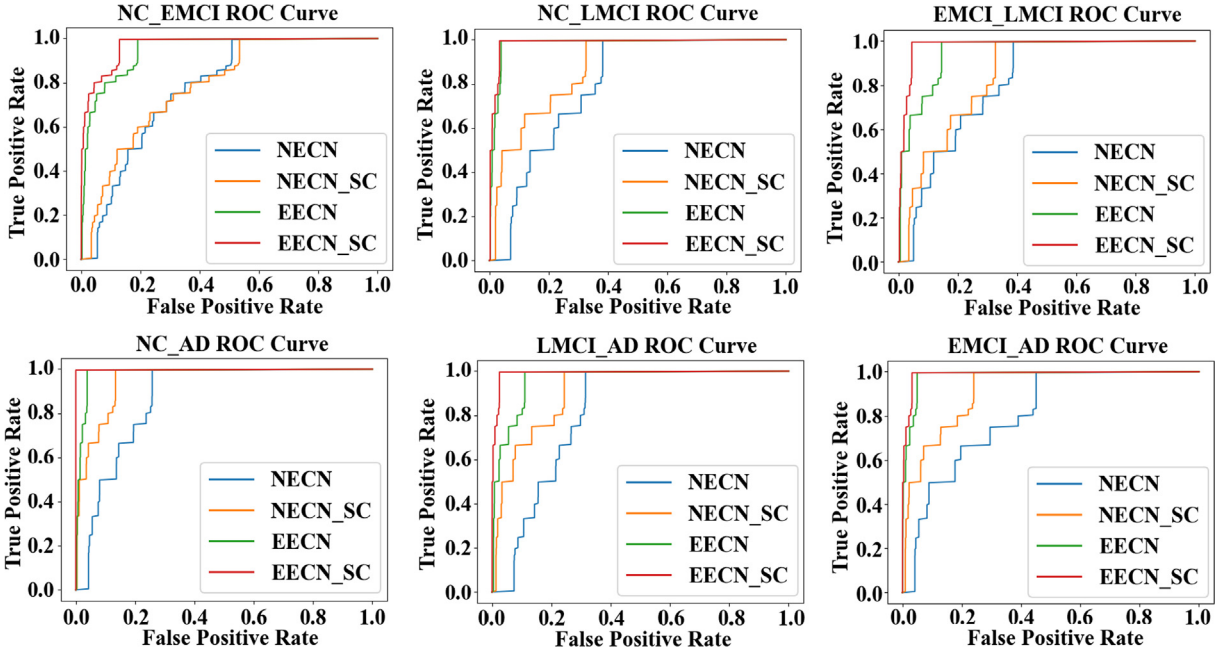

Fig. 3. ROC curves of different ECN construction methods on six classification tasks.

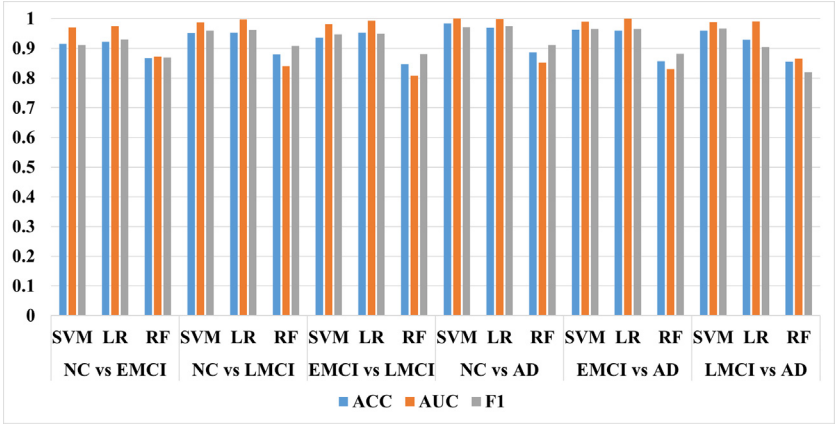

Fig. 4. The performance of different classifiers using EECN_SC for six classification tasks.

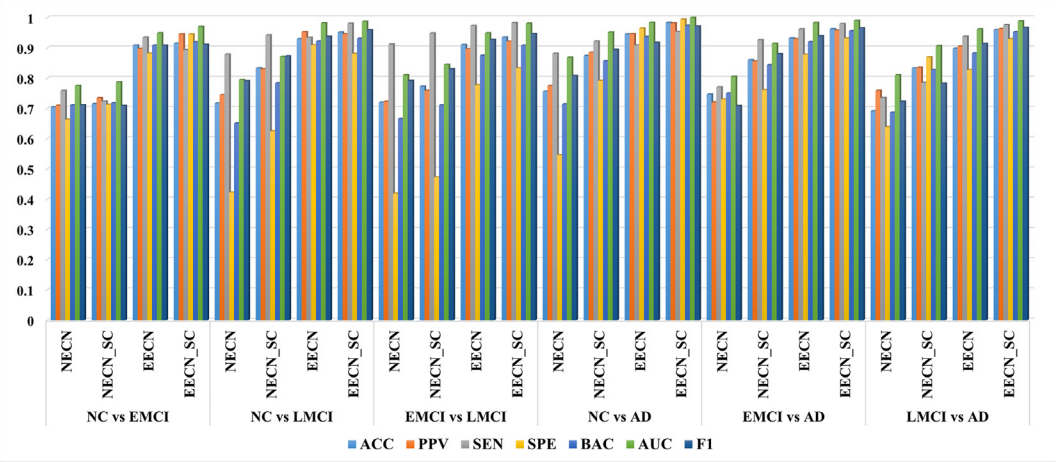

Fig. 5. Performance comparison among the methods using different ECNs for six classification tasks.

Table 4
The performance of different classifiers using EECN for six classification tasks.

Task	Method	ACC	PPV	SEN	SPE	BAC	AUC	F1
NC vs EMCI	SVM	0.9152	**0.9457**	0.8937	**0.9454**	0.9196	0.9705	0.9108
	LR	**0.9218**	0.9284	**0.9447**	0.8825	0.9136	**0.9741**	**0.9294**
	RF	0.8679	0.8453	**0.9212**	0.8231	0.8722	0.8725	0.8695
NC vs LMCI	SVM	**0.9518**	**0.9464**	0.9808	**0.8812**	**0.931**	**0.9871**	**0.9596**
	LR	**0.9531**	**0.9507**	**0.9811**	**0.8868**	**0.934**	**0.9967**	**0.9621**
	RF	0.8798	0.8555	0.9842	0.6784	0.8313	0.8404	0.9079
EMCI vs LMCI	SVM	0.9353	**0.9217**	**0.983**	**0.8333**	0.9082	0.9812	0.9468
	LR	**0.9529**	**0.9761**	**0.9311**	**0.9738**	**0.9524**	**0.9928**	**0.9489**
	RF	0.8472	0.8171	0.9773	0.6325	0.8049	0.808	0.8813
NC vs AD	SVM	**0.9839**	**0.982**	0.9537	**0.9945**	**0.9741**	**1**	0.9718
	LR	0.9695	0.9597	0.9945	0.9214	0.958	0.9982	**0.9743**
	RF	**0.8866**	**0.8529**	**0.9965**	**0.6932**	**0.8449**	**0.8515**	**0.9113**
EMCI vs AD	SVM	**0.9626**	**0.9585**	0.9798	**0.9319**	**0.9558**	0.9904	0.9656
	LR	0.9599	0.9405	**1**	0.8814	0.9407	**0.9996**	**0.9657**
	RF	0.8568	0.8277	0.9679	0.6863	0.8271	0.8303	0.8825
LMCI vs AD	SVM	**0.9601**	**0.9634**	**0.9762**	**0.9298**	**0.953**	**0.9886**	**0.9669**
	LR	0.9288	0.9002	0.9369	0.9113	0.9241	**0.9913**	0.9047
	RF	0.8558	0.8468	0.844	0.8702	0.8571	0.8653	0.8194

The value of EECN reflects the transmission of the connection fluctuation from two brain regions to the other two brain regions, indicating the causal transmission relationship between them. As can be seen from Fig. 6, the NC group has strong coordination and information transmission ability. In the EMCI stage, the overall EECN connection is relatively weaker than that in the NC group, but there are still some strong causal connections. With the gradual deterioration of the disease, after reaching the stage of LMCI, the information transmission between some brain regions is significantly weakened, and there are signs of connection loss. However, in the AD group, the ability of information transmission between some brain regions is weakened more significantly and some EECN

Table 5
Comparison with recent algorithms related to early diagnosis of AD.

Method	NC vs EMCI					NC vs LMCI					EMCI vs LMCI				
	ACC	SEN	SPE	AUC	F1	ACC	SEN	SPE	AUC	F1	ACC	SEN	SPE	AUC	F1
[32]	0.9090	0.9040	0.914	0.967	-	-	-	-	-	-	0.898	0.876	0.9140	0.9400	-
[33]	0.7431	0.7059	0.7759	-	0.72	0.7802	0.8235	0.725	-	0.8077	0.7347	0.8276	0.6	-	0.7869
[34]	0.9116	0.8255	0.957	-	-	0.9422	0.9277	0.957	-	-	0.9246	0.9397	0.8953	-	-
[35]	0.8522	0.909	0.7954	0.8982		0.8902	0.8947	0.8863	0.9288		0.8658	0.921	0.8181	0.9426	
[36]	0.925	0.95	0.90	0.98	-	-	-	-	-	-	-	-	-	-	-
[37]	0.8798	-	-	-	-	-	-	-	-	-	0.9014	-	-	-	-
ours	0.9152	0.8937	0.9454	0.9705	0.9108	0.9518	0.9808	0.8812	0.9871	0.9596	0.9353	0.983	0.8333	0.9812	0.9468
Method	**EMCI vs AD**					**NC vs AD**					**LMCI vs AD**				
	ACC	SEN	SPE	AUC	F1	ACC	SEN	SPE	AUC	F1	ACC	SEN	SPE	AUC	F1
[36]	0.865	0.88	0.85	0.94	-	0.93	0.93	0.93	0.99	-	-	-	-	-	-
[37]	-	-	-	-	-	0.9571	-	-	-	-	0.9005	-	-	-	-
[38]	-	-	-	-	-	0.8884	0.8955	0.8825	0.9022	-	-	-	-	-	-
ours	0.9626	0.9798	0.9319	0.9904	0.9657	0.9839	0.9537	0.9945	1	0.9718	0.9601	0.9762	0.9298	0.9886	0.9669

values are close to 0. However, some connections are also enhanced, which may be related to the compensatory mechanism of the human brain [39]. Taken together, it could be that as the disease worsens, the brain atrophy is severely damaged. It weakens the transmission of information between brain regions, leading to a decline in cognitive function. From the perspective of the disease stage, the EECN of EMCI and NC groups is more similar, while LMCI and AD are more similar. Therefore, timely detection and treatment of the condition at or before the EMCI stage may play an extremely important role in the deterioration of the condition into AD. This experiment also proves the necessity of early diagnosis of AD.

In Fig. 6, we observe that with the worsening of the disease, the causal relationship of information transmission between connections of some brain regions is gradually weakened or even missing. These damaged connections may play a key role in finding important indicators for the early diagnosis of AD. In fact, at the time of the feature extraction step, these important connections have been selected for feature classification. In order to better infer which brain connections might be important indicators, we analyze the characteristics used for classification. Since the classification features use the side causal connection between ROI-ROI, each feature should have two ROI-ROI connections. Therefore, the selected features have a high dimension and cannot be well mapped to the real brain template, so the features need to be further disassembled. First, the feature index corresponds to the specific ROI-ROI, and then we carry out a statistical analysis of its occurrence times and visualize it in Fig. 7. The horizontal and vertical coordinates in Fig. 7 (a) represent the index of ROI, corresponding to the 12 brain regions selected at the beginning of the experiment, and the value represents the number of occurrences of the corresponding ROI sequence pairs in the classification features. Blue indicates the number of occurrences is 0, green indicates the number of occurrences is 1, and yellow indicates the number of occurrences is 2. And we plot their distribution in the real brain in Fig. 7 (b). Finally, we count 6 ROI-ROI connections with high frequency in early diagnostic tasks for AD based on EECN method, and display them in Table 6.

As shown in Table 4, some ROI-ROI connections such as L.Lingual gyrus - R.Precental gyrus, L.Middle occipital gyrus - L.Lingual

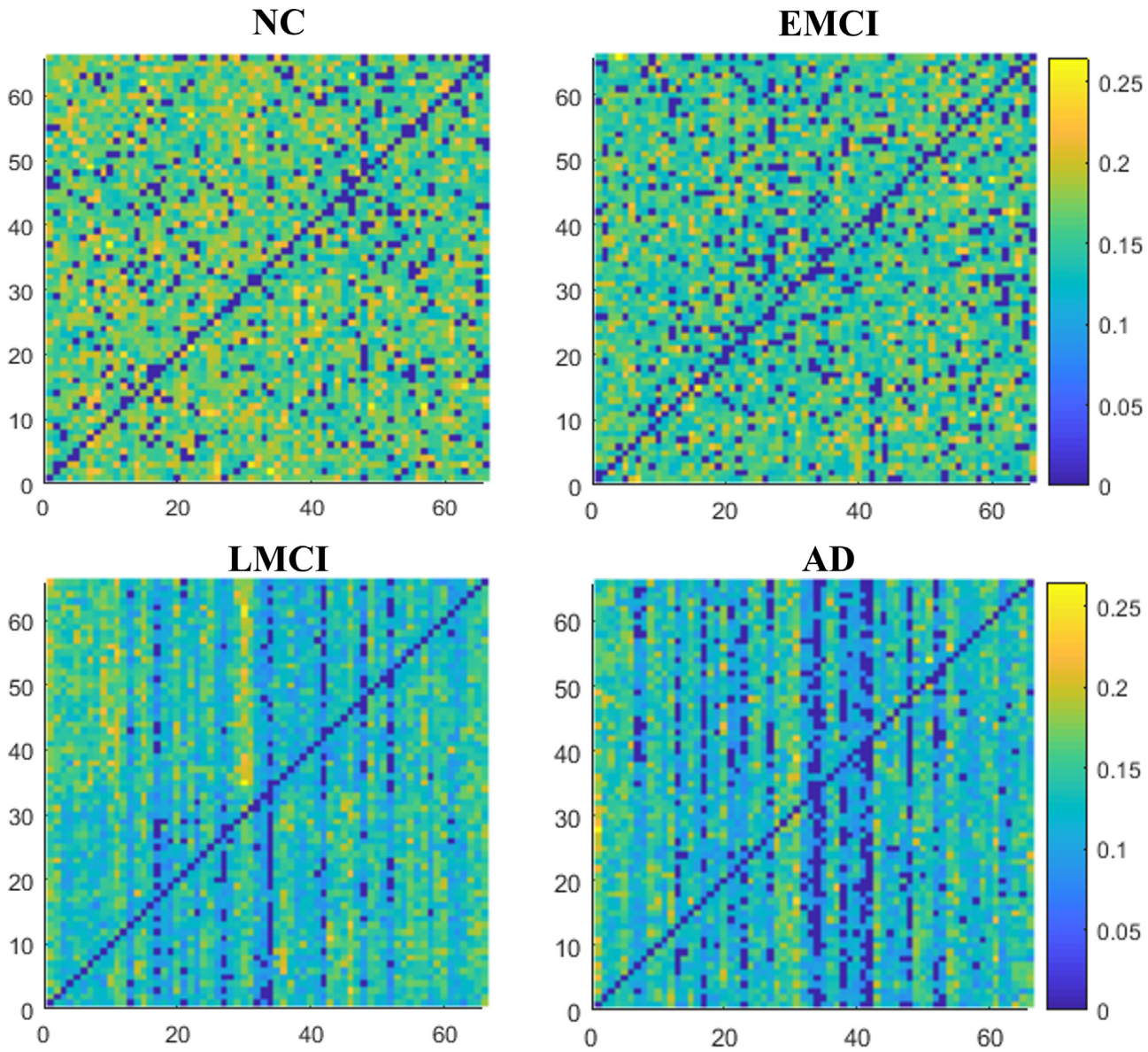

Fig. 6. The average EECNs of NC, EMCI, LMCI, and AD groups. The X-axis and Y-axis both mean the indexes of ROI-ROI.

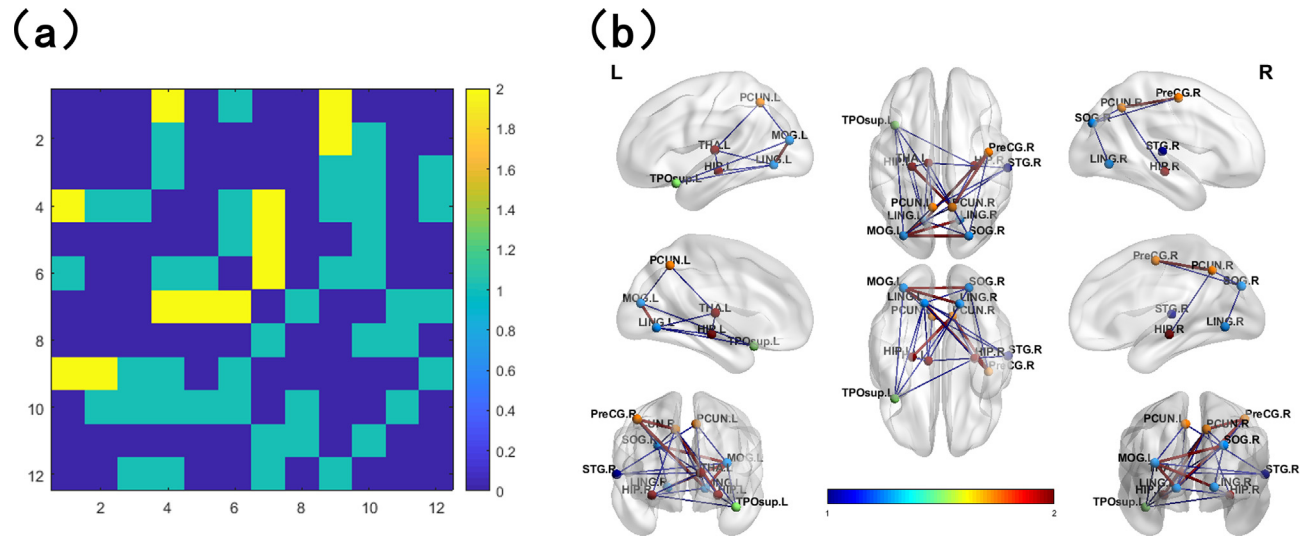

Fig. 7. (a) Analyze the features used by EECN for classification and disassemble some ROI-ROI connections. The X and Y coordinates correspond to the ROI index selected at the beginning of the experiment, and the value represents the occurrence times of the corresponding ROI-ROI connection. (b) The distribution of these ROI-ROI connections in the real brain, with the more frequent ones represented by the red line.

Table 6
The six most important ROI-ROI connections counted in early diagnostic tasks for AD based on the EECN method.

No.	ROI-ROI
1	L.Lingual gyrus - R.Precental gyrus
2	L.Middle occipital gyrus - L.Lingual gyrus
3	L.Middle occipital gyrus - R.Lingual gyrus
4	L.Middle occipital gyrus - R.Superior occipital gyrus
5	R.Precuneus - R.Precental gyrus
6	R.Precuneus - L.Hippocampus

gyrus, L.Middle occipital gyrus - R.Lingual gyrus, L.Middle occipital gyrus - R.Superior occipital gyrus, R.Precuneus - R.Precental gyrus, and R.Precuneus - L.Hippocampus seem more crucial in the early diagnosis of AD. Among them, the Lingual gyrus is related to visual signal processing, as well as logical analysis and visual memory. The Precental gyrus is the locus of the primary motor cortex, which controls behavioral movement. The Middle occipital gyrus is associated with spatial perception around the human body, and these areas have been reported in many studies on the early diagnosis of AD [40–44]. In addition, the Hippocampus plays a role in short-term and long-term memory, as well as spatial orientation. Studies have shown that AD patients have hippocampus damage, memory decline, and loss of orientation perception [45,46].

5. Conclusion

In this paper, we first improve the traditional CGC method and then propose a new edge-centric ECN construction framework. This method provides us with important information about the onset of AD from the perspective of ROI-ROI connections fluctuation causal information, which is more in line with the characteristics of biological interpretability. Finally, based on the data of ADNI, we apply this method to the classification tasks of AD, LMCI, EMCI, and NC, and achieved good results. These experiments demonstrate the effectiveness of the proposed method.

However, this paper has some shortcomings, such as not constructing EECN at the whole brain level for analysis. The main reason is the dimension size of the EECN. The number of EECN nodes is $N(N-1)/2$, which means that if too many brain regions are selected, it may lead to a dimension explosion when constructing features. Therefore, our future work can be expanded by constructing accurate EECNs at the whole brain level and then processing ultra-high dimensional features. In addition, some work related to neural networks that could integrate low-level details with higher-level semantic features [47] can also be combined with brain networks, which may produce some meaningful research works. In conclusion, the work in this paper may play a positive role in the diagnosis of brain diseases and the development of brain connection networks in the future.

Data availability

The authors do not have permission to share data.

Declaration of Competing Interest

The authors declare that they have no known competing financial interests or personal relationships that could have appeared to influence the work reported in this paper.

Acknowledgments

This work was supported in part by Ministry of Industry and Information Technology special fund for high-quality development under Grant TC220A04A-182, in part by the National Natural Science Foundation of China under Grant 62271045, in part by the National Science Fund for Distinguished Young Scholarship of China under Grant 62025602, in part by the Fundamental Research Funds for the Central Universities under Grant QNXM20220038, in part by the Science and Technology Innovation Special Foundation of Foshan Municipal People's Government under Grant BK21BFO01, in part by the Innovation and Transformation Foundation of Peking University Third Hospital under Grant BYSYZHKC2021107, in part by Key Technology Research and Development Program of Science and Technology-Scientific and Technological Innovation Team of Shaanxi Province under Grant No. 2020TD-013, in part by Key Program for International Science and Technology Cooperation Projects of China under Grant 2022YFE0112300, and in part by the XPLORER PRIZ.

References

[1] B. Dubois, N. Villain, G.B. Frisoni, G.D. Rabinovici, M. Sabbagh, S. Cappa, A. Bejanin, S. Bombois, S. Epelbaum, M. Teichmann, et al., Clinical diagnosis of alzheimer's disease: recommendations of the international working group, The Lancet Neurology 20 (2021) 484–496.

[2] A. Association, alzheimer's disease facts and figures, Alzheimer's & dementia 15 (2019) (2019) 321–387.

[3] M. Zvěřová, Clinical aspects of alzheimer's disease, Clinical biochemistry 72 (2019) 3–6.

[4] H. Taheri Gorji, N. Kaabouch, A deep learning approach for diagnosis of mild cognitive impairment based on mri images, Brain sciences 9 (2019) 217.

[5] K. Ka et al., The effect of anatomical localization of lung tumors and their correlations to the other variables on staging of lung cancer by using whole body pet/ct images, Anatomy: International Journal of Experimental & Clinical Anatomy 13 (2019).

[6] N. Zeng, H. Qiu, Z. Wang, W. Liu, H. Zhang, Y. Li, A new switching-delayed-pso-based optimized svm algorithm for diagnosis of alzheimer's disease, Neurocomputing 320 (2018) 195–202.

[7] T. Jitsuishi, A. Yamaguchi, Searching for optimal machine learning model to classify mild cognitive impairment (mci) subtypes using multimodal mri data, Scientific Reports 12 (2022) 1–14.

[8] N. Zeng, H. Li, Y. Peng, A new deep belief network-based multi-task learning for diagnosis of alzheimer's disease, Neural Computing and Applications (2021) 1–12.

[9] P.J. Drew, Vascular and neural basis of the bold signal, Current Opinion in Neurobiology 58 (2019) 61–69.

[10] D. Papo, J.M. Buldú, S. Boccaletti, E.T. Bullmore, Complex network theory and the brain, Philosophical Transactions of the Royal Society B: Biological Sciences 369 (2014) 20130520.

[11] O. Sporns, D.R. Chialvo, M. Kaiser, C.C. Hilgetag, Organization, development and function of complex brain networks, Trends in cognitive sciences 8 (2004) 418–425.

[12] S. Oldham, A. Fornito, The development of brain network hubs, Developmental cognitive neuroscience 36 (2019).

[13] B. Ibrahim, S. Suppiah, N. Ibrahim, M. Mohamad, H.A. Hassan, N.S. Nasser, M.I. Saripan, Diagnostic power of resting-state fmri for detection of network connectivity in alzheimer's disease and mild cognitive impairment: A systematic review, Human brain mapping 42 (2021) 2941–2968.

[14] K. Zhao, Q. Zheng, M. Dyrba, T. Rittman, A. Li, T. Che, P. Chen, Y. Sun, X. Kang, Q. Li, et al., Regional radiomics similarity networks reveal distinct subtypes and abnormality patterns in mild cognitive impairment, Advanced Science 9 (2022) 2104538.

[15] L. Zhang, L. Wang, J. Gao, S.L. Risacher, J. Yan, G. Li, T. Liu, D. Zhu, A.D.N. Initiative, et al., Deep fusion of brain structure-function in mild cognitive impairment, Medical image analysis 72 (2021).

[16] J. Faskowitz, F.Z. Esfahlani, Y. Jo, O. Sporns, R.F. Betzel, Edge-centric functional network representations of human cerebral cortex reveal overlapping system-level architecture, Nature neuroscience 23 (2020) 1644–1654.

[17] H.-J. Park, K. Friston, Structural and functional brain networks: from connections to cognition, Science 342 (2013) 1238411.

[18] L. Zhao, W. Zeng, Y. Shi, W. Nie, Dynamic effective connectivity network based on change points detection, Biomedical Signal Processing and Control 72 (2022).

[19] S. Dang, S. Chaudhury, B. Lall, P.K. Roy, Tractography-based score for learning effective connectivity from multimodal imaging data using dynamic bayesian networks, IEEE Transactions on Biomedical Engineering 65 (2017) 1057–1068.

[20] J. Ji, J. Liu, A. Zou, A. Zhang, Acoec-fd: Ant colony optimization for learning brain effective connectivity networks from functional mri and diffusion tensor imaging, Frontiers in Neuroscience 13 (2019) 1290.

[21] A. Roebroeck, E. Formisano, R. Goebel, Mapping directed influence over the brain using granger causality and fmri, Neuroimage 25 (2005) 230–242.

[22] L. Faes, G. Nollo, S. Stramaglia, D. Marinazzo, Multiscale granger causality, Physical Review E 96 (2017).

[23] P.A. Stokes, P.L. Purdon, A study of problems encountered in granger causality analysis from a neuroscience perspective, Proceedings of the national academy of sciences 114 (2017) E7063–E7072.

[24] D. Rangaprakash, M.N. Dretsch, A. Venkataraman, J.S. Katz, T.S. Denney Jr, G. Deshpande, Identifying disease foci from static and dynamic effective connectivity networks: illustration in soldiers with trauma, Human brain mapping 39 (2018) 264–287.

[25] T.W. Anderson, The statistical analysis of time series, John Wiley & Sons, 2011.

[26] C.R. Jack Jr, M.A. Bernstein, N.C. Fox, P. Thompson, G. Alexander, D. Harvey, B. Borowski, P.J. Britson, J.L. Whitwell, C. Ward, et al., The alzheimer's disease neuroimaging initiative (adni): Mri methods, Journal of Magnetic Resonance Imaging: An Official Journal of the International Society for, Magnetic Resonance in Medicine 27 (2008) 685–691.

[27] N. Tzourio-Mazoyer, B. Landeau, D. Papathanassiou, F. Crivello, O. Etard, N. Delcroix, B. Mazoyer, M. Joliot, Automated anatomical labeling of activations in spm using a macroscopic anatomical parcellation of the mni mri single-subject brain, Neuroimage 15 (2002) 273–289.

[28] C.-G. Yan, X.-D. Wang, X.-N. Zuo, Y.-F. Zang, Dpabi: data processing & analysis for (resting-state) brain imaging, Neuroinformatics 14 (2016) 339–351.

[29] P.A. Mundra, J.C. Rajapakse, Svm-rfe with mrmr filter for gene selection, IEEE transactions on nanobioscience 9 (2009) 31–37.

[30] S. Nusinovici, Y.C. Tham, M.Y.C. Yan, D.S.W. Ting, J. Li, C. Sabanayagam, T.Y. Wong, C.-Y. Cheng, Logistic regression was as good as machine learning for predicting major chronic diseases, Journal of clinical epidemiology 122 (2020) 56–69.

[31] T. Han, D. Jiang, Q. Zhao, L. Wang, K. Yin, Comparison of random forest, artificial neural networks and support vector machine for intelligent diagnosis of rotating machinery, Transactions of the Institute of Measurement and Control 40 (2018) 2681–2693.

[32] Y. Li, J. Liu, Y. Jiang, Y. Liu, B. Lei, Virtual adversarial training-based deep feature aggregation network from dynamic effective connectivity for mci identification, IEEE transactions on medical imaging 41 (2021) 237–251.

[33] Z. Xia, T. Zhou, S. Mamoon, A. Alfakih, J. Lu, A structure-guided effective and temporal-lag connectivity network for revealing brain disorder mechanisms, IEEE Journal of Biomedical and Health Informatics (2023).

[34] X. Song, F. Zhou, A.F. Frangi, J. Cao, X. Xiao, Y. Lei, T. Wang, B. Lei, Multi-center and multi-channel pooling gcn for early ad diagnosis based on dual-modality fused brain network, IEEE Transactions on Medical Imaging (2022).

[35] X. Song, F. Zhou, A.F. Frangi, J. Cao, X. Xiao, Y. Lei, T. Wang, B. Lei, Graph convolution network with similarity awareness and adaptive calibration for disease-induced deterioration prediction, Medical Image Analysis 69 (2021).

[36] N.J. Herzog, G.D. Magoulas, Brain asymmetry detection and machine learning classification for diagnosis of early dementia, Sensors 21 (2021) 778.

[37] Z. Fan, J. Li, L. Zhang, G. Zhu, P. Li, X. Lu, P. Shen, S.A.A. Shah, M. Bennamoun, T. Hua, et al., U-net based analysis of mri for alzheimer's disease diagnosis, Neural Computing and Applications 33 (2021) 13587–13599.

[38] J. Gan, Z. Peng, X. Zhu, R. Hu, J. Ma, G. Wu, Brain functional connectivity analysis based on multi-graph fusion, Medical image analysis 71 (2021).

[39] H. Viruega, M. Gaviria, Functional weight of somatic and cognitive networks and asymmetry of compensatory mechanisms: Collaboration or divergency among hemispheres after cerebrovascular accident?, Life 11 (2021) 495

[40] Z. Shi, X. Cao, J. Hu, L. Jiang, X. Mei, H. Zheng, Y. Chen, M. Wang, J. Cao, W. Li, et al., Retinal nerve fiber layer thickness is associated with hippocampus and lingual gyrus volumes in nondemented older adults, Progress in Neuro-Psychopharmacology and Biological Psychiatry 99 (2020).

[41] Q. Behfar, S.K. Behfar, B. Von Reutern, N. Richter, J. Dronse, R. Fassbender, G.R. Fink, O.A. Onur, Graph theory analysis reveals resting-state compensatory mechanisms in healthy aging and prodromal alzheimer's disease, Frontiers in aging neuroscience 12 (2020).

[42] I.M. McDonough, S.B. Festini, M.M. Wood, Risk for alzheimer's disease: A review of long-term episodic memory encoding and retrieval fmri studies, Ageing Research Reviews 62 (2020).

[43] T. Timmers, R. Ossenkoppele, E.E. Wolters, S.C. Verfaillie, D. Visser, S.S. Golla, F. Barkhof, P. Scheltens, R. Boellaard, W.M. Van Der Flier, et al., Associations between quantitative [18 f] flortaucipir tau pet and atrophy across the alzheimer's disease spectrum, Alzheimer's research & therapy 11 (2019) 1–12.

[44] X.-A. Bi, Q. Shu, Q. Sun, Q. Xu, Random support vector machine cluster analysis of resting-state fmri in alzheimer's disease, PloS one 13 (2018).

[45] T. Berger, H. Lee, A.H. Young, D. Aarsland, S. Thuret, Adult hippocampal neurogenesis in major depressive disorder and alzheimer's disease, Trends in Molecular Medicine 26 (2020) 803–818.

[46] J. Xue, H. Guo, Y. Gao, X. Wang, H. Cui, Z. Chen, B. Wang, J. Xiang, Altered directed functional connectivity of the hippocampus in mild cognitive impairment and alzheimer's disease: a resting-state fmri study, Frontiers in aging neuroscience 11 (2019) 326.

[47] P. Wu, Z. Wang, B. Zheng, H. Li, F.E. Alsaadi, N. Zeng, Aggn: Attention-based glioma grading network with multi-scale feature extraction and multi-modal information fusion, Computers in Biology and Medicine 152 (2023).

Shunqi Zhang received the bachelor's degree in 2020, and he is currently pursuing the M.E. degree from University of Science and Technology Beijing, China. His current research interests is medical image processing of Alzheimer's disease.

Haiyan Zhao is MD, associate chief physician of the Department of Neurology, Peking University Third Hospital. She has specialized in the basic and clinical research of neurodegenerative diseases.

Weiping Wang received the Ph.D. degree in telecommunications physics electronics from Beijing University of Posts and Telecommunications, Beijing, China, in 2015. She is currently a Professor with the Department of Computer and Communication Engineering, University of Science and Technology Beijing. She received the National Natural Science Foundation of China, the Postdoctoral fund, and the basic scientific research project. Her current research interests include brain-like computing, complex network, nonlinear system control.

Zhen Wang is a Professor with the School of Artificial Intelligence, Optics and Electronics (iOPEN), Northwestern Polytechnical University, Xi'an, China. He received the Ph.D. degree from Hong Kong Baptist University, Hong Kong, in 2014. His current research interests include complex networks, evolutionary game, and data science.

Xiong Luo received the Ph.D degree in computer applied technology from Central South University, Changsha, China, in 2004. He is currently a Professor with the School of Computer and Communication Engineering, University of Science and

Technology Beijing, Beijing, China. His current research interests include neural networks, machine learning, and computational intelligence.

Alexander Hramov is the head of Department 'Automatization, Control and Mechatronics' and the leading scientist in Research and Education Center 'Nonlinear Dynamics of Complex Systems'. His main topics are: automatic recognition and analysis of EEG and MEG signals, prevention of epileptic diseases by means of electric stimulation, design of brain-computer interfaces, synchronization in neuronal networks of brain, modelling of epilepsy. He is author and co-author of more than 100 papers in scientific journals, several monographs, and he is a head of many scientific projects and grants. He is also member of national and international societies in his field of expertise.

Jurgen Kurths studied mathematics with the University of Rostock and received the Ph.D. degree from the GDR Academy of Sciences in 1983. He was a Full Professor with the University of Potsdam from 1994 to 2008. He has been a Professor of nonlinear dynamics with Humboldt University, Berlin, and the Chair of the research domain transdisciplinary concepts of the Potsdam Institute for Climate Impact Research since 2008 and a SixthCentury Chair of Aberdeen University, U.K., since 2009. He has authored over 500 papers that are cited over 18000 times (h-factor: 57). His primary research interests include synchronization, complex networks, and time series analysis and their applications. He is a fellow of the American Physical Society. He became a member of the Academia Europaea in 2010 and the Macedonian Academy of Sciences and Arts in 2012. He received the Alexander von Humboldt Research Award from CSIR, India, in 2005, and an Honorary Doctorate from the Lobachevsky University Nizhny Novgorod in 2008 and one from the State University Saratov in 2012. He is an Editor of journals, such as PLoS ONE, the Philosophical Transaction of the Royal Society A, the Journal of Nonlinear Science, and Chaos